$Ce_xZr_{1-x}O_2$ Supported CrO_x Catalysts for CO_2-Assisted Oxidative Dehydrogenation of Propane – Probing the Active Sites and Strategies for Enhanced Stability

Jian Dou,[1] Joey Funderburg,[1] Kunran Yang,[1] Junchen Liu,[1] Kui Zhang,[2] Adam P. Harvey,[2] Vasudev P. Haribal,[3] S. James. Zhou,[3] and Fanxing Li[1,]*

[1]Department of Chemical and Biomolecular Engineering, North Carolina State University, Raleigh, NC 27606 (USA)

[2]School of Engineering, Newcastle University, Newcastle upon Tyne NE1 7RU, UK

[3]Susteon Inc., 5001 Weston Pkwy, Cary, NC 27513 (USA)

*fli5@ncsu.edu

KEYWORDS: oxidative dehydrogenation, CO_2 conversion, stability enhancement, propylene

ABSTRACT: CO_2 assisted oxidative dehydrogenation of propane (CO_2-ODH) represents an attractive approach for propylene production and CO_2 utilization. As a soft oxidant, CO_2 can minimize over-oxidation of the hydrocarbons to enhance the propylene selectivity while increasing the equilibrium yield. However, a major challenge of CO_2-ODH is the rapid deactivation of the catalysts. The current study focuses on designing $Ce_xZr_{1-x}O_2$ mixed oxide supported CrO_x catalysts for CO_2-ODH with enhanced product selectivity and catalyst stability. By doping 0-30% Ce in the $Ce_xZr_{1-x}O_2$ mixed oxide support, propane conversion of 53-79% was achieved at 600°C, with

propylene selectivity up to 82%. Compared to pure ZrO_2 supported catalyst (i.e., 5 wt.%Cr/ZrO_2), 20-30 %Ce doped catalysts (i.e., 5 wt.%Cr/$Ce_{0.2}Zr_{0.8}O_2$ and 5 wt.%Cr/$Ce_{0.3}Zr_{0.7}O_2$) inhibited the formation of CH_4 and ethylene, and improved propylene selectivity from 57 to 77-82%. Detailed characterizations of the 5%Cr/$Ce_{0.2}Zr_{0.8}O_2$ catalyst and density functional theory (DFT) calculations indicated that Cr^{3+} is the active species during the CO_2-ODH reaction, and the reaction follows a non-redox dehydrogenation pathway. Coke formation was determined to be the primary reason for catalyst deactivation, and addition of Ce to the ZrO_2 support greatly enhanced coke resistance, leading to superior stability. Coke removal by oxidizing the catalyst with air is also effective restoring its activity.

INTRODUCTION

Propylene (C_3H_6) is one of the most produced chemicals worldwide. It finds a variety of important applications such as the production of polypropylene, propylene oxide, acrylic acid, and acrylonitrile. The global propylene market is projected to exceed 165 million tons by the end of 2030.[1] Currently, propylene is mainly produced by two industrial processes: steam cracking of naphtha/liquid petroleum gas and fluid catalytic cracking of heavy gas oils. The cracking reactions are endothermic and energy intensive, so they indirectly lead to the emission of large amounts of greenhouse gases (i.e., CO_2). Direct dehydrogenation of propane is an alternative route for propylene production, and is currently receiving increased interest due to a surplus of shale gas supply. Several commercial technologies are available for dehydrogenation of propane to propylene, such as the Oleflex and CATOFIN processes.[2] The Oleflex process uses platinum catalysts (e.g., Pt-Sn/Al_2O_3) in moving bed reactors, while CATOFIN employs chromium oxide (CrO_x) catalysts (e.g., Cr/Al_2O_3) in fixed-bed reactors. However, direct dehydrogenation of

propane is also endothermic, requiring high energy input and, dehydrogenation catalysts suffer from fast deactivation due to coke deposition.

Oxidative dehydrogenation (ODH) of propane is a promising alternative to the aforementioned processes. Using oxygen as the oxidant, the oxidative dehydrogenation reaction is exothermic and its conversion is not limited by thermodynamic equilibrium. In addition, coke formation is substantially suppressed in the presence of oxygen. However, oxygen is a strong oxidant, which tends to over-oxidize the hydrocarbons (e.g., propylene) to form CO_2, limiting the yield of propylene. Chemical looping oxidative dehydrogenation has also been explored to increase propylene selectivity and eliminate the oxygen separation. However, long-term stability of the redox catalysts have yet to be demonstrated.[3–7] More recently, soft oxidants (i.e., CO_2 and N_2O) have been used as a replacement to O_2 in oxidative dehydrogenation of propane. For example, CO_2 has been shown to maintain an oxidative environment while greatly reducing over-oxidation of propylene to undesired CO_x byproducts. There are several advantages of using CO_2 as the oxidant in dehydrogenation of propane: CO_2 can react with hydrogen via reverse water gas shift reaction (RWGS) and shift the reaction equilibrium to produce more propylene. CO_2 can also enhance catalyst stability by removing formed coke via the reverse Boudouard reaction. An additional benefit to CO_2-assisted oxidative dehydrogenation of propane (CO_2-ODH) is the direct use of a greenhouse gas to mitigate CO_2 emissions. CO_2-ODH of propane[8–10] has received significantly less attention than CO_2-ODH of ethane[11–19]

Many heterogeneous catalysts based on redox active metal oxides (i.e., chromium oxide, vanadium oxide, and iron oxide) and main group metal oxides (i.e., gallium oxide) have been investigated for oxidative dehydrogenation of propane. Among the metal oxide catalysts, Cr-based catalysts have been reported to be amongst the most promising for the CO_2-ODH reaction. For

example, mesoporous silica (i.e., MCM-41) supported metal oxides exhibit activity in the following order: Cr > Ga > Ni, V > Fe, Mn, Co for CO_2-ODH.[20] In fact, CrO_x is the key component of the industrial catalyst used in the CATOFIN® process for direct dehydrogenation of propane to propylene. High dispersion of CrO_x on catalyst supports is critical in achieving high propane conversions.[21] Various mesoporous silicas with high surface areas, such as SBA-1, SBA-15, MCM-41, and MSU have been used to disperse CrO_x, and significantly higher propylene yields have been reported, compared to conventional amorphous silica-supported CrO_x catalysts.[20,22,23] Modification of CrO_x catalysts by a dopant is another strategy to improve catalyst performance. For example, a nickel-doped chromium catalyst exhibited 50% enhancement of propane conversion, due to stabilized Cr^{3+} by doped Ni.[24] Similar promotional effects were also observed for a Ru-promoted Cr catalyst with a two-fold enhancement in propylene production rate.[25]

Chromium-based catalysts are among the most active catalysts for the CO_2-assisted oxidative dehydrogenation reaction.[23,26–28] However, poor catalyst stability remains as the main obstacle for practical implementation of the CO_2-ODH process. A commonly proposed deactivation pathway is coke deposition, while other factors such as sintering and/or reduction of active sites have also been proposed as the potential causes. The presence of CO_2 can enhance catalyst stability depending on the type of catalyst support used. It was reported that both propylene yield and catalyst stability were improved using CO_2 with 5%Cr/SiO_2 catalyst, although CO_2 had no significant impact on catalyst performance for activated carbon supported CrO_x catalyst. Mixed results were observed for 5%Cr/Al_2O_3, with decreased propylene yield and improved stability in the presence of CO_2.[29] The effect of catalyst support on Cr catalyst stability has been investigated using Cr supported on mesoporous SiO_2 (i.e., SBA-15), γ-Al_2O_3, and ZrO_2.[30] Although a significant amount of research has been published on CrO_x-based catalysts for CO_2-ODH of

propane, there is still ongoing debate in terms of (i) the active sites and reaction pathway and (ii) primary deactivation mechanism. Typically, fresh CrO_x catalysts consists of both Cr^{6+} and Cr^{3+} species, which have been investigated for ODH reaction.[31] However, oxidation states of Cr *during* the ODH reaction remain unclear . *In-situ* XAS studies suggest that Cr^{6+} is reduced to Cr^{3+} in the presence of propane, which represents the active sites during direct dehydrogenation of propane without oxidants.[26] Reduction of Cr^{6+} to Cr^{3+} was also observed by *in-situ* XAS for CO_2-assisted ODH over a Cr-MCM-41 catalyst. As regeneration of Cr^{3+} to Cr^{6+} was achieved by introducing O_2 or CO_2, it was postulated that a Cr^{6+}/Cr^{3+} redox couple is responsible for the CO_2-ODH reaction.[20] Regeneration of the reduced Cr^{4+} to Cr^{6+} by CO_2 was very slow compared to O_2-assisted regeneration. Michorczyk et al., reported that reduction of Cr^{6+} to Cr^{3+} occurs during CO_2-ODH reaction for Cr/SBA-1 catalyst, as evidenced by *in-situ* UV-vis diffuse reflectance spectroscopy.[32] However, Cr^{3+}/Cr^{2+} was considered to be responsible for dehydrogenation reaction. These studies, based on either Cr^{6+}/Cr^{3+} or Cr^{3+}/Cr^{2+} redox pathway, proposed that the reaction follows a Mars-Van Krevelen mechanism. On the other hand, Hakuli et al., proposed that the dehydrogenation reaction uses both reduced Cr^{6+}, i.e., redox 3+, and exposed non-redox Cr^{3+} sites.[33] Shishido et al., further pointed out that oxidative dehydrogenation over Cr^{6+} takes place in the initial stage, while direct dehydrogenation over Cr^{3+} proceeds after 5 min of reaction.[34] After all, direct dehydrogenation of propane proceeds well over Cr^{3+} active sites.[2,35,36] In terms of the catalyst deactivation, the reduction of Cr^{6+}[20,24] and/or coke deposition[23,26,37] were proposed to be the primary mechanism.

Given these challenges in the field of CO_2-ODH with Cr catalysts and the lack of consensus over the reaction pathway and catalyst deactivation mechanism, this work aims to develop CrO_x based catalysts with enhanced selectivity/stability and investigate the underlying reaction/deactivation

mechanisms. Comprehensive characterization including both *ex-situ* and *in-situ* techniques shed light on the active sites of $CrO_x/Ce_xZr_{1-x}O_2$ catalysts. The correlations among catalyst properties, product selectivities, and stability are thus established. DFT calculations were performed to provide insights on the reaction pathways, catalyst activity, byproduct formation, and catalyst deactivation mechanism.

METHODS

Catalyst Synthesis. A sol-gel method is used for catalyst preparation to ensure a higher degree of homogeneity among the active metal and the support. Respective amounts of nitrate precursors were dissolved in deionized water (DIW) and stirred well for 15 min at room temperature, followed by the addition of citric acid. After the solution was allowed to thoroughly mix for 30 min, ethylene glycol was added dropwise and brought to 80°C until the gel formed. The resultant sol-gel product was dried at 120°C overnight then calcined at 650°C for 8 hr to burn off the organic template. Lastly, the samples were crushed, pressed at 15 MPa, and sieved to a grain size of 150 – 250 μm.

Characterization. Nitrogen adsorption/desorption isotherms at -196°C were measured using a Micromeritics ASAP 2020 porosimeter. After degassing, the respective support and catalyst (~250 mg) specific surface areas were calculated by Brunauer–Emmett–Teller (BET) analysis. Standard powder X-ray diffraction (XRD) patterns were acquired with a PANalytical Empyrean XRD over a 20-70° 2θ range, 0.05° step size, and 2°/s scan rate. The resultant data were analyzed in Microsoft Excel, while reference patterns were accessed via HighScore Plus's highly comprehensive database. X-ray photoelectron spectra (XPS) were acquired with a Kratos Analytical Axis Ultra spectrometer equipped with an Al Kα (hν = 1.487 eV) X-ray source. Thermogravimetric analysis (TGA) was performed with a TA Instruments SDT-Q600 Simultaneous TGA / DSC.

Approximately 10 mg of fresh sample was pretreated at 650ºC for 60 min under 10% O_2/Ar gas flow to drive off surface H_2O. The sample was then allowed to cool to room temperature in an argon environment. Temperature programed reduction (TPR) was completed by heating the pretreated sample to 700ºC at 20ºC/min under 10% H_2/Ar. Temperature programmed oxidation (TPO) was then immediately carried out after TPR and subsequent cooling. The TPO conditions included a 20ºC/min ramp to 700ºC under 10% O_2/Ar. Spent catalysts were analyzed via TGA by heating from room temperature to 600ºC at 20ºC/min under 10% O_2/Ar gas flow. Raman spectra were acquired using Horiba XploRA PLUS Confocal Raman Microscope with excitation source of 785 nm. *In-situ* diffuse reflectance infrared Fourier transform spectroscopy (DRIFTS) experiments were performed in a Thermal Scientific Nicolet iS50 FTIR spectrometer equipped with a high temperature cell and with a mercury-cadmium-telluride (MCT-A) detector which was cooled with liquid nitrogen. Spectra were acquired at a resolution of 4 cm^{-1} , typically over 256 scans. The catalyst was first oxidized in a 10% O_2 flow (50 mL/min) at 650ºC for 30 min and cooled

Catalytic activity measurements. Firstly, 200 mg of catalyst was loaded in a quartz U-tube with an inner diameter for 4 mm and placed in a tube-furnace after packing the ends of the U-tube with quartz wool. To create a carbon balance basis, a room temperature measurement of reactant gasses (C_3H_8:CO_2:Ar=1:2:37, 20 ml/min) was acquired. To activate the catalyst, the temperature of the furnace was ramped from room temperature to 600℃ and held at this temperature for 30 min. The activation feedstock concentration contained 10% O_2 (Ar balance) at 20 ml/min. During a 10 min argon purge, the reactor was cooled to 500℃. The reaction was then initiated by introducing relative concentrations of C_3H_8:CO_2:Ar=1:2:37 at a total flowrate of 20 ml/min. After equilibrating for 5 min, effluent gas was collected for 10 min. The reactor was then ramped to 550ºC and 600ºC

after similar equilibrations and collections. Each sample was collected via gas bag and subsequently analyzed in GC/TCD-FID instrumentation. For the stability test, the catalyst was loaded into the reactor and activated by the same procedure outlined in above. After a 10 min Ar purge at 600^{o}C, the reactant feedstock was introduced to the system at the same relative concentration and flow rate as mentioned in section 2.3 above. After flowing for 5 min to account for any pre-equilibration effects, the first gas sample was collected and designated as the 5 min sample. Samples were then collected in 30 min intervals for 180 min total time on stream. Each sample was collected for 10 min via gas bag and subsequently analyzed in GC/TCD-FID instrumentation.

Computational details. In this work, density functional theory (DFT) calculations were performed by Vienna *ab initio* simulation package (VASP).[38–41] We used the generalized gradient approximation (GGA) to calculate the electronic structures, and the Perdew-Burke-Ernzerhof (PBE) functional was employed.[42] The projector-augmented wave (PAW) method was utilized to describe the electron-core interaction.[43,44] The cutoff energy was set as 450 eV. Force threshold was set as 0.05 eV Å^{-1} with energy convergence criterion for every electronic loop of 10^{-4} eV, and these settings are proved to be accurate enough and applied in our previous work.[45,46] Spin polarization effects were considered, and Hubbard U corrections were involved with U_{eff} = 4.5 and 3.5 eV for Cr and Ce, respectively.[47,48] The lattice parameters of ZrO_2 were optimized and they were used to build a 9-layer ZrO_2(101) surface. The bottom 3 layers of the atoms were fixed during all of the calculations and the other atoms were relaxed. Based on the ZrO_2(101) surface structure, we compared the energetics when a surface Zr atom or subsurface Zr atom was substituted by Ce, and the Ce was favorably doped at surface Zr site. The Ce dopant concentration is 17%, consistent with the experimental Ce concentration of 20 %. The obtained structures were shown in Figure

S1. To further consider ODH reactions, we build 2×3 ZrO_2(101) supercell structure either with and without Ce dopant, and we further put a Cr_2O_3 cluster on the ZrO_2(101) surface. The vacuum layer was set larger than 12 Å to diminish the artificial interactions from adjacent slabs. The obtained Cr/ZrO_2 and Cr/$Ce_{0.2}Zr_{0.8}O_2$ structures were optimized by using 2 × 2 × 1 k-point grid to describe the surface Brillouin Zone. To validatethe stability of the Cr/ZrO_2 and Cr/$Ce_{0.2}Zr_{0.8}O_2$ structures, we conducted structural relaxations by *ab initio* molecular dynamics method using the parameters reported in previous work,[49,50] and it was found that the structures remain stable after 5 ps at 600ºC, suggesting good stability. The transition-state structures were obtained by climbing image nudged elastic band (CI-NEB).[51,52]

RESULTS AND DISCUSSION

Catalyst Preparation and Characterization. The 5 wt.%Cr/$CeZrO_2$ catalysts were synthesized by a one-pot sol-gel method as described in the experimental section, followed by calcination in air at 650ºC for 6 h. The structures of the catalysts were characterized by powder X-ray diffraction (Figure 1). Pure ZrO_2 supported Cr catalyst exhibits a tetragonal ZrO_2 phase. By doping 10-30 mol% Ce, the tetragonal ZrO_2 phase was retained, while peak shifts to lower angles were observed due to lattice expansion caused by Ce doping. At higher Ce loading (i.e., 50 mol%), the crystal structure changes to cubic phase, resembling that of a CeO_2 support.

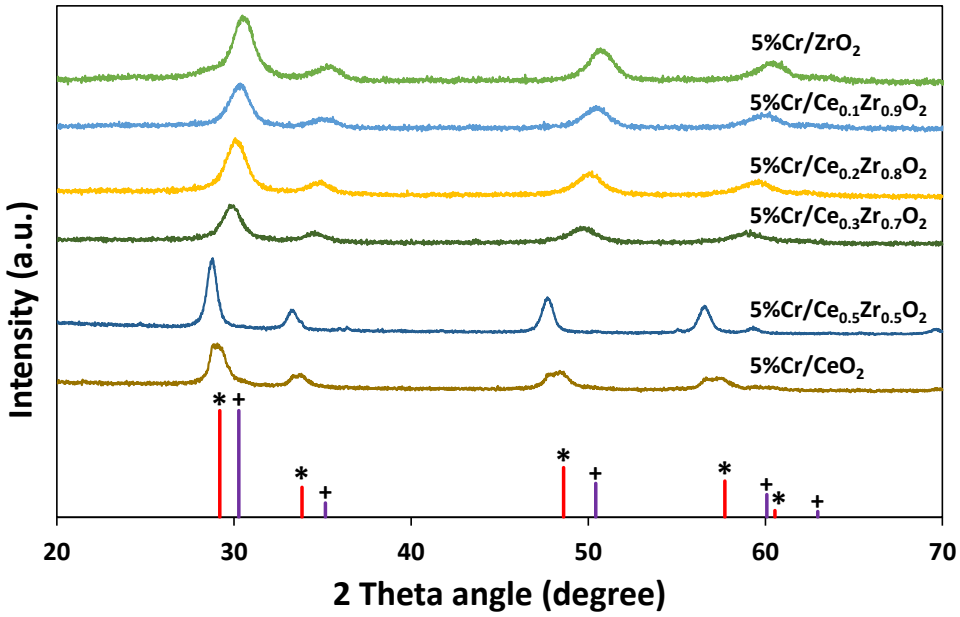

Figure 1. X-ray diffraction patterns of 5 wt.%Cr/$Ce_xZr_{1-x}O_2$ catalysts with reference of cubic CeO_2 (*) and tetragonal ZrO_2 (+) phases.

The surface areas of the 5 wt.%Cr/$Ce_xZr_{1-x}O_2$ catalysts were measured by nitrogen physisorption. As shown in Table 1, the pure ZrO_2 supported CrO_x has a BET surface area of 99.5 m^2/g. By increasing Ce doping from 0 to 100%, the surface area decreases from 99.5 to 30.3 m^2/g.

Table 1. BET surface area of 5 wt.%Cr/$Ce_xZr_{1-x}O_2$ catalysts.

Catalyst	**BET surface area (m^2/g)**
5 wt.%Cr/ZrO_2	99.5
5 wt.%Cr/$Ce_{0.1}Zr_{0.9}O_2$	89.4
5 wt.%Cr/$Ce_{0.2}Zr_{0.8}O_2$	77.1
5 wt.%Cr/$Ce_{0.3}Zr_{0.7}O_2$	58.0
5 wt.%Cr/$Ce_{0.5}Zr_{0.5}O_2$	25.2
5 wt.%Cr/CeO_2	30.3

CO_2 Assisted Oxidative Dehydrogenation of Propane. The catalytic performance of 5 wt.%Cr/$Ce_xZr_{1-x}O_2$ catalysts was evaluated for CO_2 assisted oxidative dehydrogenation of propane (Figure 2 and Table 2). Generally, both the propane and CO_2 conversion increase with reaction temperature for all the 5 wt.%Cr/$Ce_xZr_{1-x}O_2$ catalysts investigated. For example, the propane and CO_2 conversions were 13.3 and 5.0% at 500°C for 5 wt.%Cr/ZrO_2 catalyst. By increasing the reaction temperature to 550°C, the propane and CO_2 conversions increased to 42.7 and 16.8 accordingly. Further increasing the temperature to 600°C resulted in 79.8% propane conversion, and 42.7% CO_2 conversion. Although high propane conversion can be achieved at 600°C with ZrO_2-supported catalysts (i.e., 5 wt.%Cr/ZrO_2), the propylene selectivity was only at 57.6% (Table 2). By doping 10 mol% Ce in the catalyst (i.e., 5 wt.%Cr/$Ce_{0.1}Zr_{0.9}O_2$), the propane conversion slightly decreased to 75.0%, while the propylene selectivity increased to 66.7% at 600°C. Further increasing Ce doping to 20 mol% resulted in propylene selectivity reaching 79.4% with propane conversion of 62.6%. Propylene selectivity up to 92.9% can be achieved with 5 wt.%Cr/$Ce_{0.5}Zr_{0.5}O_2$ catalyst at a propane conversion of 9.7%. Overall, maximum propylene yield of ~50% is achieved with 10-20% mol Ce-doped catalysts (i.e., 5 wt.%Cr/$Ce_{0.1}Zr_{0.9}O_2$ and 5 wt.%Cr/$Ce_{0.2}Zr_{0.8}O_2$). The hydrocarbon product distribution is shown in Figure 3. Tthe major side products are methane and ethane, from cracking of propane and/or propylene. At 600°C, the methane selectivity was 34.2% for 5 wt.%Cr/ZrO_2 catalyst. The Ce-doped catalyst (i.e., 5 wt.%Cr/$Ce_xZr_{1-x}O_2$) reduced methane selectivity by half to 17.7%, suggesting that the presence of Ce inhibits cracking products formation.

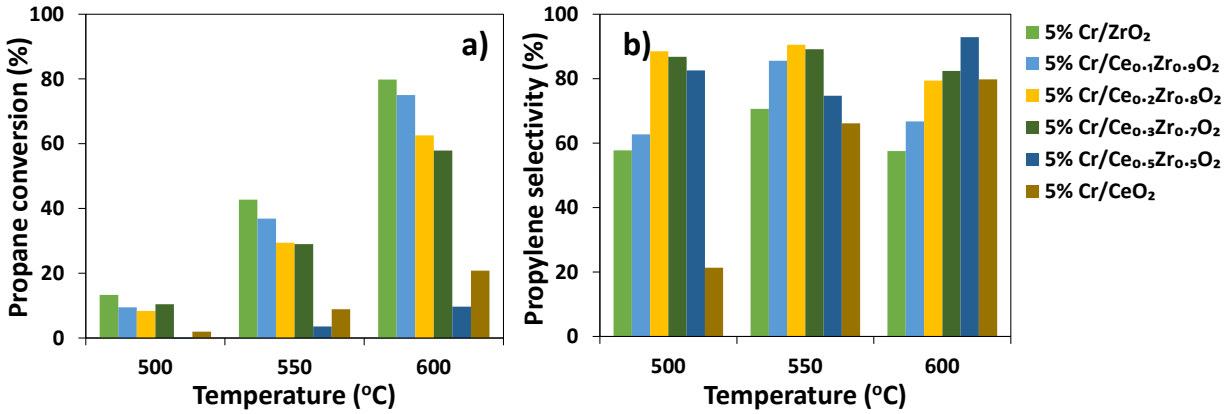

Figure 2. (a) Propane conversion, and (b) propylene selectivity for CO_2-ODH reaction over 5% $Cr/Ce_xZr_{1-x}O_2$ (x = 0, 0.1, 0.2, 0.3, 0.5, 1.0) catalysts. Reaction condition: 0.2 g catalyst, 0.5 ml/min C_3H_8, 1 ml/min CO_2, 18.5 ml/min Ar, 1 bar, 500-600°C.

Table 2. CO_2-ODH of propane performance over % $Cr/Ce_xZr_{1-x}O_2$ (x = 0, 0.1, 0.2, 0.3, 0.5, 1.0) catalysts.[a]

Sample	C_3H_8 Conv. (%)	CO_2 Conv. (%)	C_3H_6 Sel. (%)	C_3H_6 Yield (%)
5%Cr/ZrO_2	79.8	42.7	57.6	45.9
5%Cr/$Ce_{0.1}Zr_{0.9}O_2$	75.0	41.6	66.7	50.1
5%Cr/$Ce_{0.2}Zr_{0.8}O_2$	62.6	31.2	79.4	49.7
5%Cr/$Ce_{0.3}Zr_{0.7}O_2$	57.9	33.8	82.4	47.7
5%Cr/$Ce_{0.5}Zr_{0.5}O_2$	9.7	7.9	92.9	9.0
5%Cr/CeO_2	20.8	11.9	79.8	16.6
ZrO_2	6.1	0.2	82.2	5.0
$Ce_{0.2}Zr_{0.8}O_2$	4.1	5.2	78.3	3.2

[a]Reaction condition: 0.2 g catalyst, 0.5 ml/min C_3H_8, 1 ml/min CO_2, 18.5 ml/min Ar, 1 bar, 500-600°C.

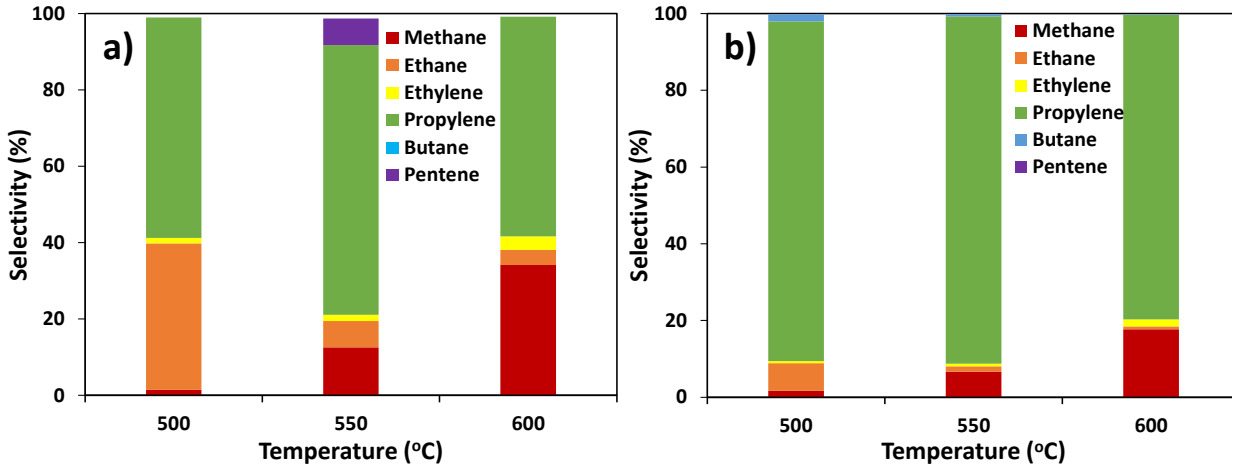

Figure 3. Product distributions for CO_2-ODH reaction over (a) 5%Cr/ZrO_2 and (b) 5% Cr/$Ce_{0.2}Zr_{0.8}O_2$ catalysts. Reaction condition: 0.5 ml/min C_3H_8, 1 ml/min CO_2, 18.5 ml/min Ar, 500°C, 550°C, and 600°C.

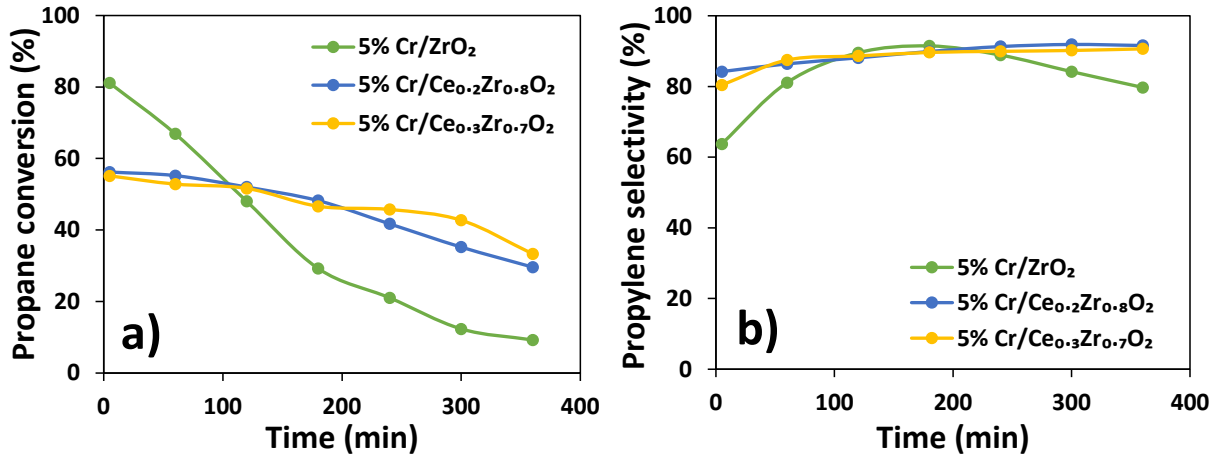

Figure 4. Stability for CO_2-ODH over 5%Cr/ZrO_2, 5%Cr/$Ce_{0.2}Zr_{0.8}O_2$, and 5% Cr/$Ce_{0.3}Zr_{0.7}O_2$ catalysts: (a) propane conversion and (b) propylene selectivity. Reaction condition: 0.5 ml/min C_3H_8, 1 ml/min CO_2, 18.5 ml/min Ar, 600°C, 6 h.

The stability of 5%Cr/ZrO_2, 5%Cr/$Ce_{0.2}Zr_{0.8}O_2$, and 5%Cr/$Ce_{0.3}Zr_{0.7}O_2$ catalysts were evaluated for CO_2-ODH reaction over 6 hours (Figure 4). The 5%Cr/ZrO_2 catalyst had a higher initial

propane conversion of 81.1% compared to 55.1-56.2% from Ce-doped catalysts (i.e., 5%Cr/$Ce_{0.2}Zr_{0.8}O_2$, and 5%Cr/$Ce_{0.3}Zr_{0.7}O_2$). However, the 5%Cr/ZrO_2 catalyst deactivated very fast, with propane conversion dropping to 48.0% at 2 h of reaction. At 6 h, the propane conversion further decreased to 9.2%, corresponding to 11% of its initial value at 5 min. As a comparison, the Ce-doped catalysts are far more stable, retaining 52-60% of their initial activity after 6 hours of CO_2-ODH reaction.

Reaction Pathway and Mechanism. Comprehensive characterizations were conducted to understand the underlying reaction mechanism. The oxidation states of Cr for the fresh and spent 5%Cr/ZrO_2 and 5%Cr/$Ce_{0.2}Zr_{0.8}O_2$ catalysts were examined by X-ray photoelectron spectroscopy (Figure 5). Both Cr^{6+} and Cr^{3+} were present in the as-prepared catalysts, with Cr^{6+}/Cr^{3+} ratio of 2.45 and 1.75 for 5%Cr/ZrO_2 and 5%Cr/$Ce_{0.2}Zr_{0.8}O_2$ catalyst, respectively. After CO_2-ODH reaction, CrO_x was reduced, and only Cr^{3+} was observed in both 5%Cr/ZrO_2 and 5%Cr/$Ce_{0.2}Zr_{0.8}O_2$ catalysts. This suggests that Cr^{3+} is the active site during the ODH reaction. The surface structure of supported CrO_x was analyzed by Raman spectroscopy (Figure 6). For as-prepared 5%Cr/ZrO_2 and 5%Cr/$Ce_{0.2}Zr_{0.8}O_2$ catalysts, three peaks were observed in the 800-1100 cm^{-1} region, corresponding to surface Cr^{6+} species.[53] More specifically, the peaks at 1028-1030 cm^{-1} are attributed to C=O vibration of isolated CrO_x species. The peaks at 880-882 and 1002-1008 cm^{-1} are due to Cr-O-Cr and Cr=O vibrations of polymeric CrO_x, respectively. The peaks corresponding to ZrO_2 or $Ce_{0.2}Zr_{0.8}O_2$ were observed in the region of 200-800 cm^{-1}, which could overlap with Ce-O-Ce stretching (i.e., 465 cm^{-1}) in the case of 5%Cr/$Ce_{0.2}Zr_{0.8}O_2$ catalyst.[54] After CO_2-ODH reaction, the peak intensity for both the monomeric and polymeric CrO_x species significantly decreased. This suggests that reduction of Cr^{6+} occurs during the reaction, consistent

with XPS results. In order to further verify this hypothesis, the fresh 5%Cr/$Ce_{0.2}Zr_{0.8}O_2$ catalyst was pre-reduced in H_2 at 350°C before conducting the CO_2-ODH reaction (Figure 7). The initial activity of the as-prepared and pre-reduced 5%Cr/$Ce_{0.2}Zr_{0.8}O_2$ catalysts were similar, with propane conversion at 56.2 and 57.1%, respectively. This further confirms that the reduced Cr^{3+} is the active species for propane dehydrogenation. It is noted that the pre-reduced catalyst was slightly less stable comparing to the fresh catalyst, with 44% of initial activity preserved at 6 h of reaction for the pre-reduced catalyst vs 53% remained for the fresh catalyst. This is likely to be due to the increased coke formation of the pre-reduced catalyst, as will be discussed later in the context of deactivation mechanism.

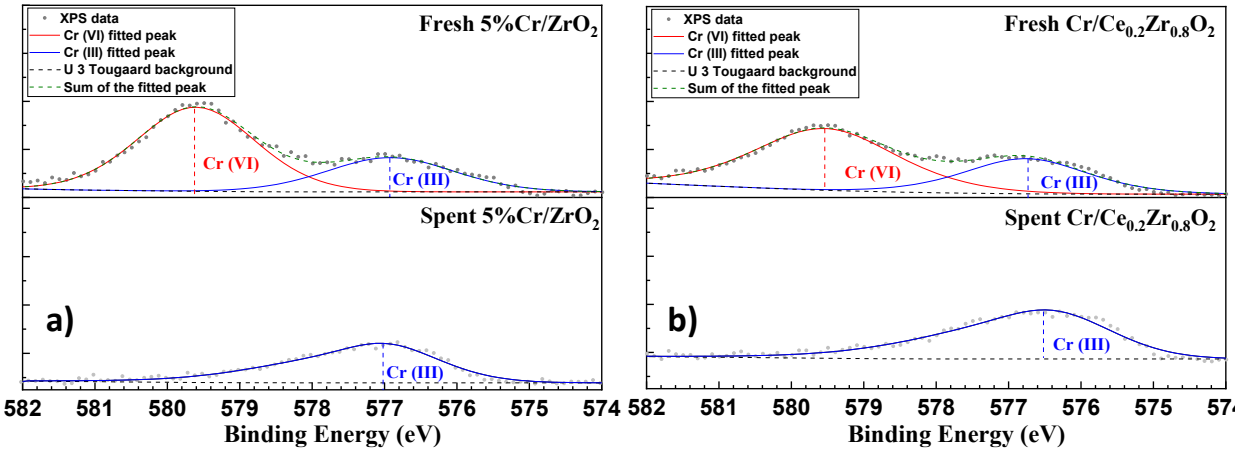

Figure 5. X-ray photoelectron spectra of Cr 2p in fresh (top) and spent (bottom) (a) 5%Cr/ZrO_2 and (b) 5%Cr/$Ce_{0.2}Zr_{0.8}O_2$ catalysts.

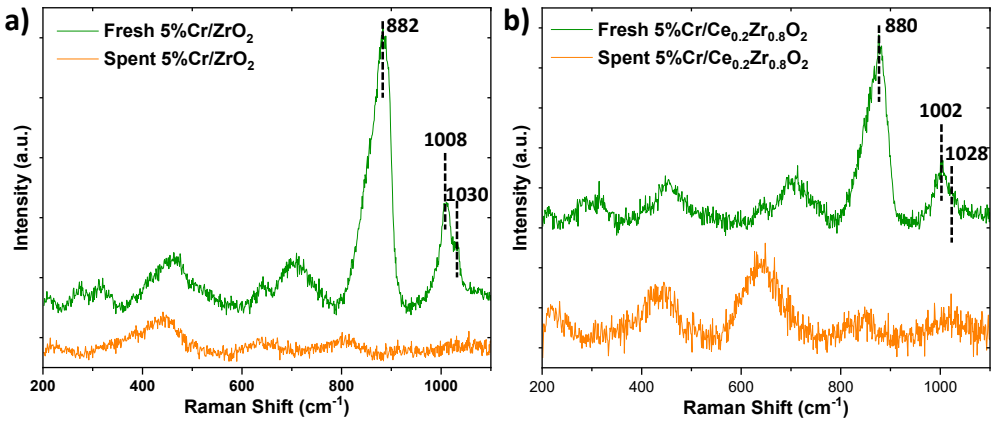

Figure 6. Raman spectra of fresh (top) and spent (bottom) (a) 5%Cr/ZrO_2 and (b) 5%Cr/$Ce_{0.2}Zr_{0.8}O_2$ catalysts.

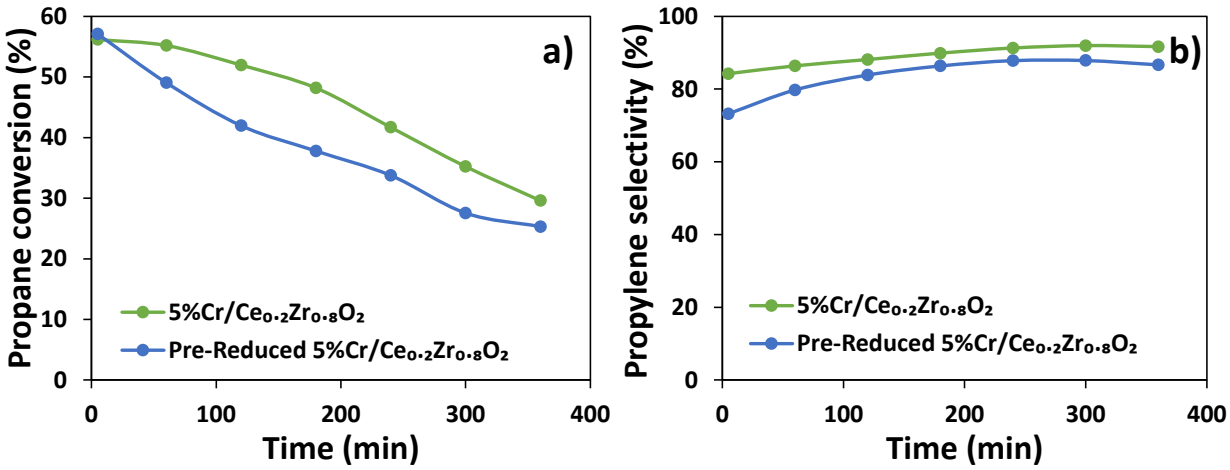

Figure 7. Stability test for CO_2-ODH reaction over fresh and pre-reduced 5%Cr/$Ce_{0.2}Zr_{0.8}O_2$ catalyst. Reduction condition: 2 ml/min H_2, 18 ml/min Ar, 350°C, 30 min. Reaction condition: 0.5 ml/min C_3H_8, 1 ml/min CO_2, 18.5 ml/min Ar, 600°C, 360 min.

In-situ DRIFTS study was carried out to provide insights on the CO_2-ODH reaction pathway over the 5%Cr/$Ce_{0.2}Zr_{0.8}O_2$ catalyst (Figure 8). The fresh catalyst was first pretreated at 650°C for 30 min the presence of 10%O_2, followed by cooling down to room temperature for propane adsorption. After propane adsorption, the catalyst was purged at room temperature for 20 min.

Adsorption of propane is evidenced by peaks at 1378 and 1456 cm^{-1}, corresponding to C-H bending. Interestingly, three peaks appear in the region of 1500-1700 cm^{-1} (i.e., 1560, 1616 and 1675 cm^{-1}) due to C=C stretching, suggesting formation of surface-adsorbed propylene. Desorption of propylene was observed when the catalyst was heated above 200°C. When propane and CO_2 were co-adsorbed on the catalyst surface, both propane and propylene peaks were observed (Figure 8b). Desorption of propylene occurs at above 200°C, similar as the case of propane adsorption only. In the temperature range studied (i.e., 25-400°C), no CO peak was observed. This suggests that propane dehydrogenation is more favorable than CO_2 splitting over the 5%Cr/$Ce_{0.2}Zr_{0.8}O_2$ catalyst. Therefore, direct dehydrogenation of propane is probably the pathway for propylene production. CO_2 can then react with the formed hydrogen via RWGS to shift the reaction equilibrium to produce more propylene as well as the CO coproduct.

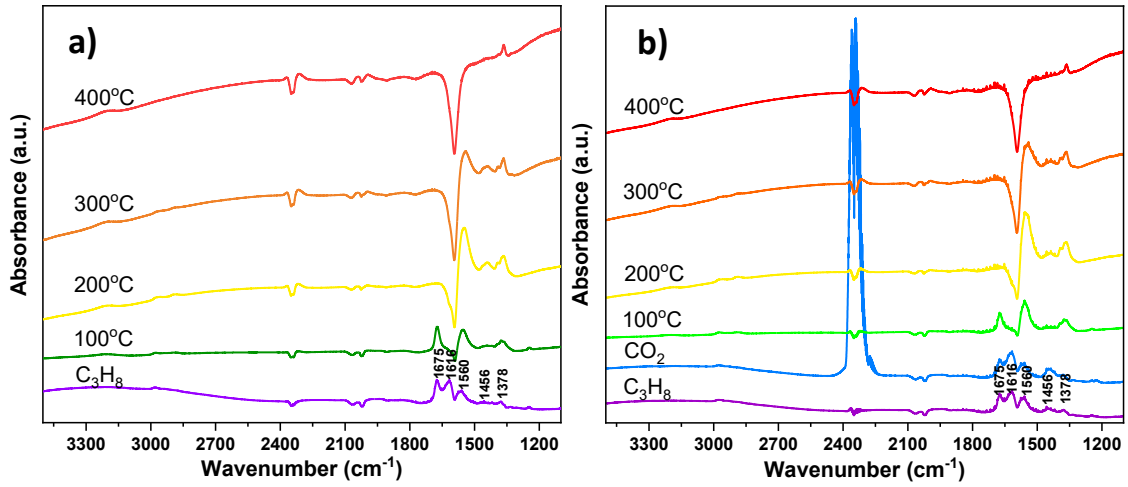

Figure 8. *In-situ* DRIFTS study of 5%Cr/$Ce_{0.2}Zr_{0.8}O_2$ catalyst in the presence of (a) propane and (b) propane + CO_2 at 25-400°C.

DFT calculations were performed to provide molecular-level insights into the CO_2-assisted ODH on Cr/ZrO_2 and Cr/$Ce_{0.2}Zr_{0.8}O_2$ catalysts. Figure 9a shows the energy profile of ODH of

propane on the two structure models considered. The ODH reaction starts from the activation of propane (C_3H_8) to isopropyl (C_3H_7) with barriers of 2.16 eV on Cr/ZrO_2 and 2.33 eV on $Cr/Ce_{0.2}Zr_{0.8}O_2$ surfaces, indicating slightly favorable kinetics on Cr/ZrO_2 for this step. The dehydrogenation of C_3H_8 to propyl ($CH_2CH_2CH_3$) is unfavorable compared with isopropyl [55] The subsequent dehydrogenation of C_3H_7 to propylene (C_3H_6) has a low barrier of 0.80 eV on Cr/ZrO_2 while the barrier is 2.12 eV on $Cr/Ce_{0.2}Zr_{0.8}O_2$ surfaces. The results suggest that Cr/ZrO_2 has better reactivity than $Cr/Ce_{0.2}Zr_{0.8}O_2$ for the dehydrogenation from C_3H_8 to C_3H_6, and the rate-limiting step is the dehydrogenation of C_3H_8 to C_3H_7. In addition, the desorption energies of C_3H_6 are 0.43 eV and 0.51 eV for Cr/ZrO_2 and $Cr/Ce_{0.2}Zr_{0.8}O_2$, respectively. Considering the dehydrogenation barriers of C_3H_6 to C_3H_5 are larger than 1.5 eV on Cr/ZrO_2 and $Cr/Ce_{0.2}Zr_{0.8}O_2$, the product C_3H_6 would be more favorable towards desorption from the surface than further dehydrogenation. In Figure 9b, the barriers and reaction energies of CO_2 splitting reaction on Cr/ZrO_2 and $Cr/Ce_{0.2}Zr_{0.8}O_2$ surfaces are calculated to be 2.58 eV and 2.43 eV, respectively. These barriers are higher than those of C_3H_8 dehydrogenation to C_3H_7, and hence the dehydrogenation reactions are likely the main reactions during the overall process, consistent with observations from DRIFTS study as well as activity measurements.

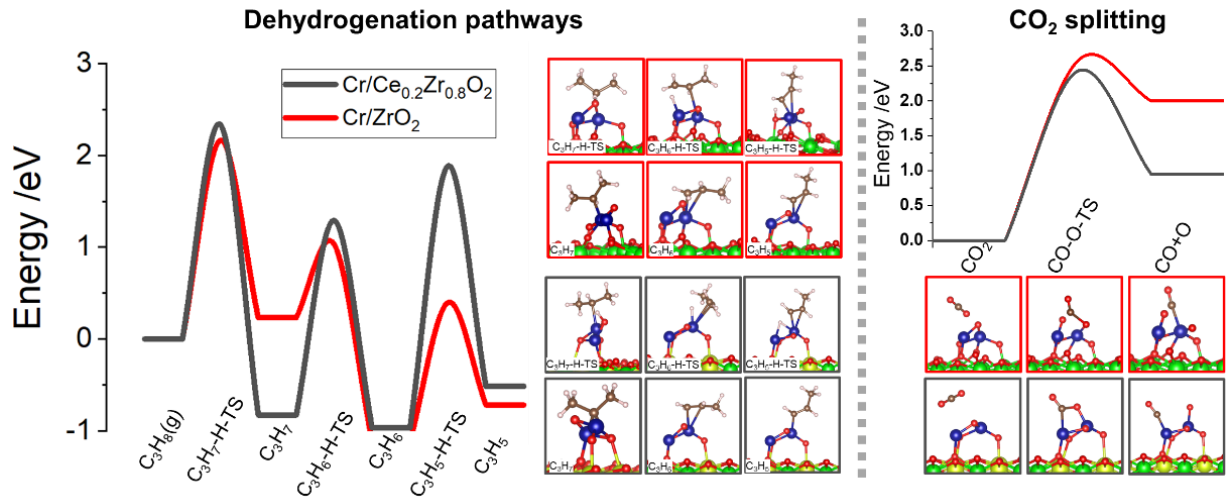

Figure 9. Energy profile of (a) ODH of propane and (b) CO_2 splitting and corresponding structures during the reaction on Cr/ZrO_2 (in red) and $Cr/Ce_{0.2}Zr_{0.8}O_2$ structures (in black). The transition states are represented by "-TS". Yellow, green, blue, brown, white and red balls represent Ce, Zr, Cr, C, H and O atoms, respectively.

Effect of Ce Doping. To further understand the superior product selectivity for $Cr/Ce_{0.2}Zr_{0.8}O_2$, we considered cracking reactions during propane dehydrogenation, which are a key precursor reaction of forming coke species, as well as methane and ethylene byproducts. As mentioned above, C_3H_6 is readily desorbed from the surface, and the C-C bond cleavage of C_3H_6 has barriers of ~3 eV on both Cr/ZrO_2 and $Cr/Ce_{0.2}Zr_{0.8}O_2$ surfaces, and hence C_3H_6 is not likely to be the precursor of cracking reactions. In addition, considering C_3H_8 species has no unpaired electrons and it binds weakly with the surface, it is unlikely for such species to undergo cracking. Therefore, here we mainly discuss the cracking process of C_3H_7 (Figure S2). According to the comparison between dehydrogenation barriers of C_3H_7 ($E_{a,\ dehydro}$) and C-C bond cleavage barriers of C_3H_7 ($E_{a,\ C\text{-}C\ cleav}$) in Table 3, it was found that C_3H_7 can be dehydrogenated to C_3H_6 on both Cr/ZrO_2 and $Cr/Ce_{0.2}Zr_{0.8}O_2$ structures. A descriptor of $E_{a,\ C\text{-}C\ cleav}$ - $E_{a,\ dehydro}$ is introduced to estimate the possibility of cracking and a lower value means C_3H_7 species tend to have higher possibility to

have C-C bond cleavage relative to further dehydrogenation. A similar descriptor was used in previous hydrogenation reaction studies.[56–59] According to the results in Table 3, C_3H_7 is much less likely to undergo C-C bond cleavage on $Cr/Ce_{0.2}Zr_{0.8}O_2$, since the $E_{a,\ C\text{-}C\ cleav} - E_{a,\ dehydro}$ value is significantly lower on Cr/ZrO_2 (0.27 eV) than on $Cr/Ce_{0.2}Zr_{0.8}O_2$ (0.88 eV). This is in accordance with the reduced coke formation and higher propylene selectivity found on 5% $Cr/Ce_{0.2}Zr_{0.8}O_2$ during the reaction (Figure 3).

Table 3. Reaction barriers of dehydrogenation of C_3H_7 ($E_{a,\ dehydro}$), C-C bond cleavage of C_3H_7 ($E_{a,\ C\text{-}C\ cleav}$) and their difference. A lower $E_{a,\ C\text{-}C\ cleav} - E_{a,\ dehydro}$ indicates higher possibility for C_3H_7 to undergo C-C bond cleavage reactions to form CH_3 and $CHCH_3$.

	Cr/ZrO_2	$Cr/Ce_{0.2}Zr_{0.8}O_2$
$E_{a,\ dehydro}$	0.80	2.12
$E_{a,\ C\text{-}C\ cleav}$	1.07	3.00
$E_{a,\ C\text{-}C\ cleav} - E_{a,\ dehydro}$	0.27	0.88

In order to understand the effect of Ce on catalyst stability, the spent $5\%Cr/ZrO_2$ and $5\%Cr/Ce_{0.2}Zr_{0.8}O_2$ catalysts were investigated by temperature programmed oxidation in $10\%O_2$. As shown in Figure 10, weight loss was observed for both catalysts, suggesting coke deposition on the catalyst during the CO_2-ODH reaction. Specifically, the spent $5\%Cr/ZrO_2$ catalyst has 5.3 wt.% coke deposited, while the Ce doped catalyst only has 2.5 wt.% coke deposition. This shows that doping of Ce inhibits coke formation, which results in enhanced catalyst stability. Furthermore, as the direct dehydrogenation of propane over Cr^{3+} active sites is the primary reaction pathway based on our experimental results and DFT calculations, the

catalyst deactivation is likely mainly caused by coke deposition, given Cr^{3+} remained after CO_2-ODH reaction.

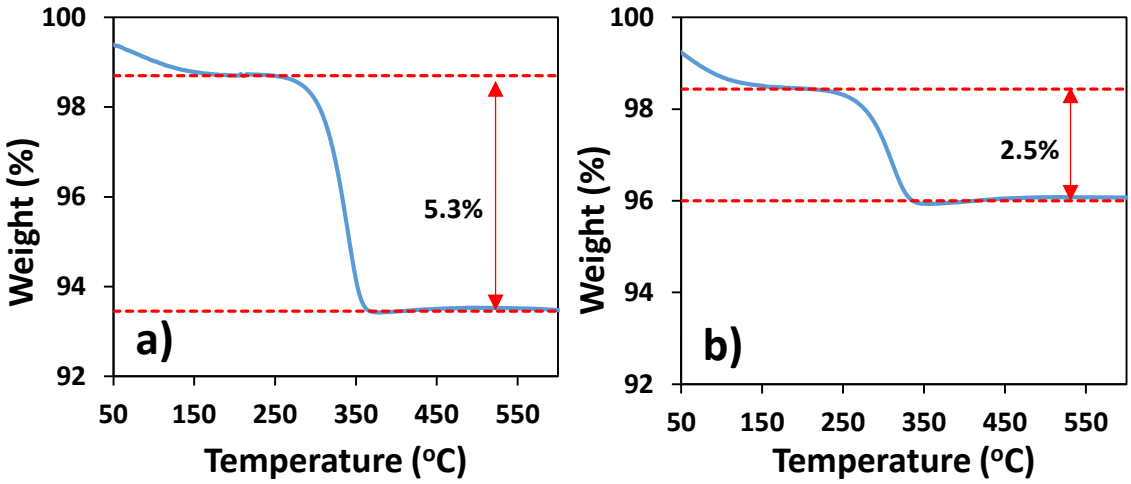

Figure 10. Temperature programed oxidation (TPO) of spent 5%Cr/ZrO_2 and 5%Cr/$Ce_{0.2}Zr_{0.8}O_2$ catalyst. Oxidation condition: 10% O_2/Ar, 200 ml/min, and 20°C/min ramp to 600°C.

CONCLUSIONS

In summary, effective $Ce_xZr_{1-x}O_2$ supported CrO_x catalysts have been developed with high selectivity and enhanced stability for CO_2-ODH of propane. Comprehensive characterizations identified that the as-prepared catalysts consist of both monomeric and polymeric CrO_x species (i.e., 6+ and 3+). Under the reaction conditions, the Cr^{6+} is easily reduced, and activity is maintained when the catalyst is pre-reduced (removing the Cr $^{6+}$), indicating that Cr^{3+} is the active site in CO_2-ODH reactions. *In-situ* DRIFTS study, coupled with DFT calculations, suggest that the reaction proceeds via a direct dehydrogenation pathway. Ce doping modifies the electronic structure of supported Cr^{3+}, increasing the energy barrier for C-C bond breakage. This inhibits the

selectivity towards byproducts. Besides the enhanced propylene selectivity, Ce doping reduces coke formation by as much as 50% compared to undoped ZrO_2 supported Cr catalyst, leading to substantially enhanced catalyst stability.

ASSOCIATED CONTENT

Supporting Information.

AUTHOR INFORMATION

Corresponding Author

*Email: fli5@ncsu.edu

Notes

The authors declare no competing financial interest.

ACKNOWLEDGMENT

This work was supported by the US Department of Energy (DE-FE0031917) and the National Science Foundation (CBET-2116724). The XPS characterizations were performed in part at the Duke University Shared Materials Instrumentation Facility (SMIF), a member of the North Carolina Research Triangle Nanotechnology Network (RTNN), which is supported by the National Science Foundation (award number ECCS-2025064) as part of the National Nanotechnology Coordinated Infrastructure (NNCI). The XRD and Raman characterizations were performed in part at the Analytical Instrumentation Facility (AIF) at North Carolina State University, which is supported by the State of North Carolina and the National Science Foundation

(award number ECCS-2025064). The AIF is a member of the North Carolina Research Triangle Nanotechnology Network (RTNN), a site in the National Nanotechnology Coordinated Infrastructure (NNCI). We acknowledge the computing resources provided by North Carolina State University High Performance Computing Services Core Facility (RRID:SCR_022168).

REFERENCES

(1) Agarwal, A.; Sengupta, D.; El-Halwagi, M. Sustainable Process Design Approach for On-Purpose Propylene Production and Intensification. *ACS Sustain. Chem. Eng.* **2018**, *6* (2), 2407–2421. https://doi.org/10.1021/acssuschemeng.7b03854.

(2) Chen, S.; Chang, X.; Sun, G.; Zhang, T.; Xu, Y.; Wang, Y.; Pei, C.; Gong, J. Propane Dehydrogenation: Catalyst Development, New Chemistry, and Emerging Technologies. *Chem. Soc. Rev.* **2021**, *50* (5), 3315–3354. https://doi.org/10.1039/D0CS00814A.

(3) Chen, S.; Pei, C.; Chang, X.; Zhao, Z.-J.; Mu, R.; Xu, Y.; Gong, J. Coverage-Dependent Behaviors of Vanadium Oxides for Chemical Looping Oxidative Dehydrogenation. *Angew. Chem. Int. Ed.* **2020**, *59* (49), 22072–22079. https://doi.org/10.1002/anie.202005968.

(4) Chen, S.; Zeng, L.; Mu, R.; Xiong, C.; Zhao, Z.-J.; Zhao, C.; Pei, C.; Peng, L.; Luo, J.; Fan, L.-S.; Gong, J. Modulating Lattice Oxygen in Dual-Functional Mo–V–O Mixed Oxides for Chemical Looping Oxidative Dehydrogenation. *J. Am. Chem. Soc.* **2019**, *141* (47), 18653–18657. https://doi.org/10.1021/jacs.9b09235.

(5) Li, X.; Cheng, D.; Zhao, Z.-J.; Chen, F.; Gong, J. Temperature-Induced Deactivation Mechanism of ZnFe2O4 for Oxidative Dehydrogenation of 1-Butene. *React. Chem. Eng.* **2017**, *2* (2), 215–225. https://doi.org/10.1039/C6RE00179C.

(6) Zhu, X.; Imtiaz, Q.; Donat, F.; Müller, C. R.; Li, F. Chemical Looping beyond Combustion – a Perspective. *Energy Environ. Sci.* **2020**, *13* (3), 772–804. https://doi.org/10.1039/C9EE03793D.

(7) Wang, X.; Gao, Y.; Krzystowczyk, E.; Iftikhar, S.; Dou, J.; Cai, R.; Wang, H.; Ruan, C.; Ye, S.; Li, F. High-Throughput Oxygen Chemical Potential Engineering of Perovskite Oxides for Chemical Looping Applications. *Energy Environ. Sci.* **2022**. https://doi.org/10.1039/D1EE02889H.

(8) Gomez, E.; Xie, Z.; Chen, J. G. The Effects of Bimetallic Interactions for CO2-Assisted Oxidative Dehydrogenation and Dry Reforming of Propane. *AIChE J.* **2019**, *65* (8), e16670. https://doi.org/10.1002/aic.16670.

(9) Jiang, X.; Sharma, L.; Fung, V.; Park, S. J.; Jones, C. W.; Sumpter, B. G.; Baltrusaitis, J.; Wu, Z. Oxidative Dehydrogenation of Propane to Propylene with Soft Oxidants via Heterogeneous Catalysis. *ACS Catal.* **2021**, *11* (4), 2182–2234. https://doi.org/10.1021/acscatal.0c03999.

(10) Gomez, E.; Yan, B.; Kattel, S.; Chen, J. G. Carbon Dioxide Reduction in Tandem with Light-Alkane Dehydrogenation. *Nat. Rev. Chem.* **2019**, *3* (11), 638–649. https://doi.org/10.1038/s41570-019-0128-9.

(11) Yan, B.; Yao, S.; Chen, J. G. Effect of Oxide Support on Catalytic Performance of FeNi-Based Catalysts for CO2-Assisted Oxidative Dehydrogenation of Ethane. *ChemCatChem* **2020**, *12* (2), 494–503. https://doi.org/10.1002/cctc.201901585.

(12) Al-Mamoori, A.; Alghamdi, T.; Rownaghi, A. A.; Rezaei, F. Enhancing the Ethylene Yield over Hybrid Adsorbent Catalyst Materials in CO2-Assisted Oxidative Dehydrogenation of Ethane by Tuning Catalyst Support Properties. *Energy Fuels* **2020**, *34* (11), 14483–14492. https://doi.org/10.1021/acs.energyfuels.0c02750.
(13) Liu, J.; Gao, Y.; Wang, X.; Li, F. Molten-Salt-Mediated Carbon Dioxide Capture and Superequilibrium Utilization with Ethane Oxidative Dehydrogenation. *Cell Rep. Phys. Sci.* **2021**, *2* (7), 100503. https://doi.org/10.1016/j.xcrp.2021.100503.
(14) Rahmani, F.; Haghighi, M.; Amini, M. The Beneficial Utilization of Natural Zeolite in Preparation of Cr/Clinoptilolite Nanocatalyst Used in CO2-Oxidative Dehydrogenation of Ethane to Ethylene. *J. Ind. Eng. Chem.* **2015**, *31*, 142–155. https://doi.org/10.1016/j.jiec.2015.06.018.
(15) Baidya, T.; van Vegten, N.; Baiker, A. Selective Conversion of Ethane to Ethene via Oxidative Dehydrogenation Over Ca-Doped ThO2 Using CO2 as Oxidant. *Top. Catal.* **2011**, *54* (13), 881. https://doi.org/10.1007/s11244-011-9696-8.
(16) Zhu, J.; Qin, S.; Ren, S.; Peng, X.; Tong, D.; Hu, C. Na2WO4/Mn/SiO2 Catalyst for Oxidative Dehydrogenation of Ethane Using CO2 as Oxidant. *Spec. Issue 10th Int. Conf. CO Util. Tianijn China May 17-21 2009* **2009**, *148* (3), 310–315. https://doi.org/10.1016/j.cattod.2009.07.074.
(17) Jin, L.; Reutenauer, J.; Opembe, N.; Lai, M.; Martenak, D. J.; Han, S.; Suib, S. L. Studies on Dehydrogenation of Ethane in the Presence of CO2 over Octahedral Molecular Sieve (OMS-2) Catalysts. *ChemCatChem* **2009**, *1* (4), 441–444. https://doi.org/10.1002/cctc.200900149.
(18) Zhao, X.; Wang, X. Oxidative Dehydrogenation of Ethane to Ethylene by Carbon Dioxide over Cr/TS-1 Catalysts. *Catal. Commun.* **2006**, *7* (9), 633–638. https://doi.org/10.1016/j.catcom.2006.02.005.
(19) Gaab, S.; Machli, M.; Find, J.; Grasselli, R. K.; Lercher, J. A. Oxidative Dehydrogenation of Ethane Over Novel Li/Dy/Mg Mixed Oxides: Structure–Activity Study. *Top. Catal.* **2003**, *23* (1), 151–158. https://doi.org/10.1023/A:1024836707308.
(20) Takehira, K.; Ohishi, Y.; Shishido, T.; Kawabata, T.; Takaki, K.; Zhang, Q.; Wang, Y. Behavior of Active Sites on Cr-MCM-41 Catalysts during the Dehydrogenation of Propane with CO2. *J. Catal.* **2004**, *224* (2), 404–416. https://doi.org/10.1016/j.jcat.2004.03.014.
(21) Ge, X.; Zou, H.; Wang, J.; Shen, J. Modification of Cr/SiO2 for the Dehydrogenation of Propane to Propylene in Carbon Dioxide. *React. Kinet. Catal. Lett.* **2005**, *85* (2), 253–260. https://doi.org/10.1007/s11144-005-0268-4.
(22) Michorczyk, P.; Ogonowski, J.; Zeńczak, K. Activity of Chromium Oxide Deposited on Different Silica Supports in the Dehydrogenation of Propane with CO2 – A Comparative Study. *J. Mol. Catal. Chem.* **2011**, *349* (1), 1–12. https://doi.org/10.1016/j.molcata.2011.08.019.
(23) Baek, J.; Yun, H. J.; Yun, D.; Choi, Y.; Yi, J. Preparation of Highly Dispersed Chromium Oxide Catalysts Supported on Mesoporous Silica for the Oxidative Dehydrogenation of Propane Using CO2: Insight into the Nature of Catalytically Active Chromium Sites. *ACS Catal.* **2012**, *2* (9), 1893–1903. https://doi.org/10.1021/cs300198u.
(24) Yun, D.; Baek, J.; Choi, Y.; Kim, W.; Lee, H. J.; Yi, J. Promotional Effect of Ni on a CrOx Catalyst Supported on Silica in the Oxidative Dehydrogenation of Propane with CO2. *ChemCatChem* **2012**, *4* (12), 1952–1959. https://doi.org/10.1002/cctc.201200397.

(25) Jin, R.; Easa, J.; Tran, D. T.; O'Brien, C. P. Ru-Promoted CO2 Activation for Oxidative Dehydrogenation of Propane over Chromium Oxide Catalyst. *Catal. Sci. Technol.* **2020**, *10* (6), 1769–1777. https://doi.org/10.1039/C9CY01990A.
(26) Santhosh Kumar, M.; Hammer, N.; Rønning, M.; Holmen, A.; Chen, D.; Walmsley, J. C.; Øye, G. The Nature of Active Chromium Species in Cr-Catalysts for Dehydrogenation of Propane: New Insights by a Comprehensive Spectroscopic Study. *J. Catal.* **2009**, *261* (1), 116–128. https://doi.org/10.1016/j.jcat.2008.11.014.
(27) Michorczyk, P.; Ogonowski, J.; Kuśtrowski, P.; Chmielarz, L. Chromium Oxide Supported on MCM-41 as a Highly Active and Selective Catalyst for Dehydrogenation of Propane with CO2. *Appl. Catal. Gen.* **2008**, *349* (1), 62–69. https://doi.org/10.1016/j.apcata.2008.07.008.
(28) Wang, J.; Zhu, M.-L.; Song, Y.-H.; Liu, Z.-T.; Wang, L.; Liu, Z.-W. Molecular-Level Investigation on Supported CrOx Catalyst for Oxidative Dehydrogenation of Propane with Carbon Dioxide. *J. Catal.* **2022**, *409*, 87–97. https://doi.org/10.1016/j.jcat.2022.03.027.
(29) Takahara, I.; Saito, M. Promoting Effects of Carbon Dioxide on Dehydrogenation of Propane over a SiO2-Supported Cr2O3 Catalyst. *Chem. Lett.* **1996**, *25* (11), 973–974. https://doi.org/10.1246/cl.1996.973.
(30) Zhang, X.; Yue, Y.; Gao, Z. Chromium Oxide Supported on Mesoporous SBA-15 as Propane Dehydrogenation and Oxidative Dehydrogenation Catalysts. *Catal. Lett.* **2002**, *83* (1), 19–25. https://doi.org/10.1023/A:1020693028720.
(31) Weckhuysen, B. M.; Schoonheydt, R. A. Alkane Dehydrogenation over Supported Chromium Oxide Catalysts. *Catal. Today* **1999**, *51* (2), 223–232. https://doi.org/10.1016/S0920-5861(99)00047-4.
(32) Michorczyk, P.; Pietrzyk, P.; Ogonowski, J. Preparation and Characterization of SBA-1–Supported Chromium Oxide Catalysts for CO2 Assisted Dehydrogenation of Propane. *Microporous Mesoporous Mater.* **2012**, *161*, 56–66. https://doi.org/10.1016/j.micromeso.2012.05.011.
(33) Hakuli, A.; Kytökivi, A.; Krause, A. O. I. Dehydrogenation of I-Butane on CrOx/Al2O3 Catalysts Prepared by ALE and Impregnation Techniques. *Appl. Catal. Gen.* **2000**, *190* (1), 219–232. https://doi.org/10.1016/S0926-860X(99)00310-5.
(34) Shishido, T.; Shimamura, K.; Teramura, K.; Tanaka, T. Role of CO2 in Dehydrogenation of Propane over Cr-Based Catalysts. *Catal. Energy Environ. Technol. 13th Korea-Jpn. Symp. Catal.* **2012**, *185* (1), 151–156. https://doi.org/10.1016/j.cattod.2011.10.028.
(35) Conley, M. P.; Delley, M. F.; Núñez-Zarur, F.; Comas-Vives, A.; Copéret, C. Heterolytic Activation of C–H Bonds on CrIII–O Surface Sites Is a Key Step in Catalytic Polymerization of Ethylene and Dehydrogenation of Propane. *Inorg. Chem.* **2015**, *54* (11), 5065–5078. https://doi.org/10.1021/ic502696n.
(36) Carter, J. H.; Bere, T.; Pitchers, J. R.; Hewes, D. G.; Vandegehuchte, B. D.; Kiely, C. J.; Taylor, S. H.; Hutchings, G. J. Direct and Oxidative Dehydrogenation of Propane: From Catalyst Design to Industrial Application. *Green Chem.* **2021**, *23* (24), 9747–9799. https://doi.org/10.1039/D1GC03700E.
(37) Silva, R. R. C. M.; Oliveira, H. A.; Guarino, A. C. P. F.; Toledo, B. B.; Moura, M. B. T.; Oliveira, B. T. M.; Passos, F. B. Effect of Support on Methane Decomposition for Hydrogen Production over Cobalt Catalysts. *Int. J. Hydrog. Energy* **2016**, *41* (16), 6763–6772. https://doi.org/10.1016/j.ijhydene.2016.02.101.

(38) Kresse, G.; Furthmüller, J. Efficiency of Ab-Initio Total Energy Calculations for Metals and Semiconductors Using a Plane-Wave Basis Set. *Comput. Mater. Sci.* **1996**, *6* (1), 15–50. https://doi.org/10.1016/0927-0256(96)00008-0.
(39) Kresse, G.; Furthmüller, J. Efficient Iterative Schemes for Ab Initio Total-Energy Calculations Using a Plane-Wave Basis Set. *Phys. Rev. B* **1996**, *54* (16), 11169–11186. https://doi.org/10.1103/PhysRevB.54.11169.
(40) Kresse, G.; Hafner, J. Ab Initio Molecular Dynamics for Liquid Metals. *Phys. Rev. B* **1993**, *47* (1), 558–561. https://doi.org/10.1103/PhysRevB.47.558.
(41) Kresse, G.; Hafner, J. Ab Initio Molecular-Dynamics Simulation of the Liquid-Metal--Amorphous-Semiconductor Transition in Germanium. *Phys. Rev. B* **1994**, *49* (20), 14251–14269. https://doi.org/10.1103/PhysRevB.49.14251.
(42) Perdew, J. P.; Burke, K.; Ernzerhof, M. Generalized Gradient Approximation Made Simple. *Phys. Rev. Lett.* **1996**, *77* (18), 3865–3868. https://doi.org/10.1103/PhysRevLett.77.3865.
(43) Blöchl, P. E. Projector Augmented-Wave Method. *Phys. Rev. B* **1994**, *50* (24), 17953–17979. https://doi.org/10.1103/PhysRevB.50.17953.
(44) Kresse, G.; Joubert, D. From Ultrasoft Pseudopotentials to the Projector Augmented-Wave Method. *Phys. Rev. B* **1999**, *59* (3), 1758–1775. https://doi.org/10.1103/PhysRevB.59.1758.
(45) Yang, K.; Zaffran, J.; Yang, B. Fast Prediction of Oxygen Reduction Reaction Activity on Carbon Nanotubes with a Localized Geometric Descriptor. *Phys. Chem. Chem. Phys.* **2020**, *22* (2), 890–895. https://doi.org/10.1039/C9CP04885E.
(46) Yang, K.; Yang, B. Identifying the Reaction Network Complexity and Structure Sensitivity of Selective Catalytic Oxidation of Ammonia over Ag Surfaces. *Appl. Surf. Sci.* **2022**, *584*, 152584. https://doi.org/10.1016/j.apsusc.2022.152584.
(47) Fabris, S.; de Gironcoli, S.; Baroni, S.; Vicario, G.; Balducci, G. Reply to ``Comment on `Taming Multiple Valency with Density Functionals: A Case Study of Defective Ceria' ' '. *Phys. Rev. B* **2005**, *72* (23), 237102. https://doi.org/10.1103/PhysRevB.72.237102.
(48) Jain, A.; Hautier, G.; Moore, C. J.; Ping Ong, S.; Fischer, C. C.; Mueller, T.; Persson, K. A.; Ceder, G. A High-Throughput Infrastructure for Density Functional Theory Calculations. *Comput. Mater. Sci.* **2011**, *50* (8), 2295–2310. https://doi.org/10.1016/j.commatsci.2011.02.023.
(49) Yang, K.; Liu, J.; Yang, B. Mechanism and Active Species in NH3 Dehydrogenation under an Electrochemical Environment: An Ab Initio Molecular Dynamics Study. *ACS Catal.* **2021**, *11* (7), 4310–4318. https://doi.org/10.1021/acscatal.0c05247.
(50) Yang, K.; Liu, J.; Yang, B. Electrocatalytic Oxidation of Ammonia on Pt: Mechanistic Insights into the Formation of N2 in Alkaline Media. *J. Catal.* **2022**, *405*, 626–633. https://doi.org/10.1016/j.jcat.2021.10.029.
(51) Henkelman, G.; Jónsson, H. Improved Tangent Estimate in the Nudged Elastic Band Method for Finding Minimum Energy Paths and Saddle Points. *J. Chem. Phys.* **2000**, *113* (22), 9978–9985. https://doi.org/10.1063/1.1323224.
(52) Henkelman, G.; Uberuaga, B. P.; Jónsson, H. A Climbing Image Nudged Elastic Band Method for Finding Saddle Points and Minimum Energy Paths. *J. Chem. Phys.* **2000**, *113* (22), 9901–9904. https://doi.org/10.1063/1.1329672.
(53) Weckhuysen, B. M.; Wachs, I. E. In Situ Raman Spectroscopy of Supported Chromium Oxide Catalysts: 18O2−16O2 Isotopic Labeling Studies. *J. Phys. Chem. B* **1997**, *101* (15), 2793–2796. https://doi.org/10.1021/jp9631011.

(54) Loridant, S. Raman Spectroscopy as a Powerful Tool to Characterize Ceria-Based Catalysts. *Perspect. Heterog. Catal. Occas. 60th Anniv. Res. Inst. Catal. CNRS Lyon-Villeubanne Fr.* **2021**, *373*, 98–111. https://doi.org/10.1016/j.cattod.2020.03.044.
(55) Zhang, R.; Chang, Q.-Y.; Ma, F.; Zeeshan, M.; Yang, M.-L.; Sui, Z.-J.; Chen, D.; Zhou, X.-G.; Zhu, Y.-A. Enhanced Catalytic Performance of Transition Metal-Doped Cr2O3 Catalysts for Propane Dehydrogenation: A Microkinetic Modeling Study. *Chem. Eng. J.* **2022**, *446*, 136913. https://doi.org/10.1016/j.cej.2022.136913.
(56) Yang, K.; Yang, B. Surface Restructuring of Cu-Based Single-Atom Alloy Catalysts under Reaction Conditions: The Essential Role of Adsorbates. *Phys. Chem. Chem. Phys.* **2017**, *19* (27), 18010–18017. https://doi.org/10.1039/C7CP02152F.
(57) Yang, K.; Yang, B. Identification of the Active and Selective Sites over a Single Pt Atom-Alloyed Cu Catalyst for the Hydrogenation of 1,3-Butadiene: A Combined DFT and Microkinetic Modeling Study. *J. Phys. Chem. C* **2018**, *122* (20), 10883–10891. https://doi.org/10.1021/acs.jpcc.8b01980.
(58) Zou, S.; Lou, B.; Yang, K.; Yuan, W.; Zhu, C.; Zhu, Y.; Du, Y.; Lu, L.; Liu, J.; Huang, W.; Yang, B.; Gong, Z.; Cui, Y.; Wang, Y.; Ma, L.; Ma, J.; Jiang, Z.; Xiao, L.; Fan, J. Grafting Nanometer Metal/Oxide Interface towards Enhanced Low-Temperature Acetylene Semi-Hydrogenation. *Nat. Commun.* **2021**, *12* (1), 5770. https://doi.org/10.1038/s41467-021-25984-8.
(59) Yang, K.; Yang, B. Addressing the Uncertainty of DFT-Determined Hydrogenation Mechanisms over Coinage Metal Surfaces. *Faraday Discuss.* **2021**, *229* (0), 50–61. https://doi.org/10.1039/C9FD00122K.